

## Investigating the removal of tetracycline antibiotic from aqueous solution using synthesized $\text{Fe}_3\text{O}_4$ @Cuttlebone magnetic nanocomposite

Mohammad Malakootian<sup>a,c</sup>, Marziyeh Ansari Shiri<sup>b,c,\*</sup>

<sup>a</sup>Environmental Health Engineering Research Center, Kerman University of Medical Sciences, Kerman, Iran, email: m\_malakootian@kmu.ac.ir/m.malakootian@yahoo.com

<sup>b</sup>Student Research Committee, Kerman University of Medical Sciences, Kerman, Iran, Tel. +98-9036096650; email: marziyehansari566@gmail.com

<sup>c</sup>Department of Environmental Health Engineering, Faculty of Public Health, Kerman University of Medical Sciences, Kerman, Iran

Received 27 July 2020; Accepted 8 January 2021

### ABSTRACT

The presence of antibiotics in aqueous media, and subsequently, their transfer to the environment and the entry of these compounds into the body of living organisms cause disturbances in living organisms and ecosystems. This study was aimed to evaluate the removal efficiency of tetracycline (TC) antibiotics from aqueous media by synthesized  $\text{Fe}_3\text{O}_4$ @Cuttlebone (Cb) magnetic nanocomposite. The  $\text{Fe}_3\text{O}_4$ @Cb magnetic nanocomposite was synthesized by co-precipitation method under green conditions and structurally investigated using the following techniques: Fourier transform infrared, field emission scanning electron microscopy, energy-dispersive X-ray spectroscopy, mapping, X-ray diffraction, Brunauer-Emmett-Teller, and vibrating-sample magnetometer. Parameters affecting removal such as pH (3–11), initial concentration of TC (4–20 mg/L), adsorbent dosage (0.05–0.25 g/L), and contact time (15–115 min) were evaluated. The response surface methodology based on central composite design was used by Design-Expert 11 software to design the experiments and find the optimal conditions. The  $\text{Fe}_3\text{O}_4$ @Cb magnetic nanocomposite was synthesized at the nanometer scale (approximately 31 nm) with magnetic properties and high specific surface area. The quadratic model was identified as the best model by the software. The  $R^2$  and  $p$  values of lack of fit were 0.9723 and 0.0535, respectively. The optimal conditions for the removal of TC were pH 5, initial TC concentration of 8 mg/L, adsorbent dosage of 0.2 g/L, and contact time of 90 min. The maximum removal efficiency of TC using  $\text{Fe}_3\text{O}_4$ @Cb magnetic nanocomposite in synthetic conditions and simulated real wastewater was 80.15% and 75.34%, respectively. The  $\text{Fe}_3\text{O}_4$ @Cb magnetic nanocomposite had an effective potential to remove TC from aqueous solution.

**Keywords:** Antibiotic; Tetracycline; Magnetic nanocomposite; Aqueous solution; Central composite design

### 1. Introduction

Pollution of water resources through emerging pollutants is increasing. Due to the population growth as well as the production and release of new compounds, emerging pollutants are very dangerous, so that some of them can disrupt enzymes and endocrine and genetic systems in humans. Antibiotics are among the emerging pollutants, and if their residues enter the body, they can cause severe

side effects [1]. Antibiotics also target some responsible organisms and destroy the ecology or the environment. Some antibiotics are non-biodegradable and remain in the environment for a long time [2].

Among the various types of antibiotics, tetracyclines (TCs) are the second most common group of antibiotics in terms of production and consumption worldwide, which are obtained naturally by fermentation of some fungi or semi-synthetic processes. Today, they are frequently used

\* Corresponding author.

to treat a variety of infectious diseases and affect gram-positive and gram-negative bacteria and to some extent of mycoplasmas and some fungi [3,4]. Absorption of TCs after consumption by humans and animals is very poor, irregular, and variable; and more than 70% of these compounds are excreted as primary and active compounds through feces and urine into domestic wastewater and ultimately lead to environmental and water pollution [5]. Due to their widespread use and higher adsorption capacity, the presence of TC antibiotics has been reported in various environmental matrices including surface water, groundwater [6], domestic wastewater [7], and soil and sediments [8,9], so conventional wastewater treatment plants are not capable of completely removing these micropollutants [10]. Techniques commonly used to remove antibiotics include ozonation [11], coagulation [12], photocatalytic degradation [13–23], ion exchange, liquid membrane separation, reverse osmosis, and adsorption. Among these techniques, adsorption is preferred due to the simplicity in design, ease of construction, high efficiency, relatively low cost, and the absence of highly toxic by-products [24].

Considering the advantages of adsorption method in removing organic and inorganic pollutants from aqueous media [25–31], the use of biocomposites as adsorbents has received great attention due to its non-toxicity, cheapness, availability, and efficient degradability [32–35]. The advantages of bio-adsorbents over conventional treatment methods include low cost, simplicity, high efficiency, low sludge production, and ease of use [36]. Cuttlebone (Cb) has been used in a number of studies as a bio-adsorbent to remove fluoride from water [37,38] and antibiotics, ibuprofen, naproxen, and carbamazepine from river water [39]. On the other hand, Cb is a material found in abundance on the shores of the Persian Gulf in Iran; hence, it is an inexpensive adsorbent that is easily available. However, using Cb as an adsorbent has some disadvantages, including time-consuming separation of it from the process medium by filtration or centrifugation methods, error due to the adsorption of some pollutant to the filter surface in the separation process by filtration, and low surface area to volume ratio of the adsorbent for adsorbing the pollutant.

Iron nanoparticles are one of the most common magnetic materials that have been widely used in water and wastewater treatment in recent years [40]. Iron nanoparticles have been employed in various studies in composite or functionalized forms to remove antibiotics such as TC, oxytetracycline, chlortetracycline, doxycycline, ciprofloxacin, erythromycin, amoxicillin, atenolol, and gemfibrozil [27,41–47]. Iron nanoparticles have advantages such as small particle size, high specific adsorption surface area, high density, high spontaneous reactivity of reactive surface sites, and easy separation from the process medium. Therefore, the disadvantages mentioned for Cb adsorbent, by compositing Cb with iron nanoparticles and magnetizing it, the disadvantages can be eliminated and its adsorption properties can be improved.

In different water and wastewater treatment methods, choosing the optimum conditions for the process is very important. The proposed methods should minimize environmental pollution and should be cost-effective

[48,49]. Typically, optimization of studies in batch reactors is performed using a traditional one-variable-at-a-time approach, but this method cannot fully demonstrate the effects of interaction between variables. In addition, it is time-consuming and requires a number of experiments to determine the optimum level. Response surface methodology (RSM) is a powerful optimization method that can be applied to optimize the response, when the response variable is influenced by several independent variables [50,51]. Central composite design (CCD) method is one of the most popular RSM. Using the response surface conditions, the CCD is employed to determine the optimum conditions of the effect of each independent variable, which is one of the most important advantages of this statistical method [48,52,53]. The CCD method has been used in various studies as a suitable optimization method [50,54].

Considering the current concerns about the presence of antibiotics, including TC, in various waters and the potential risks that these antibiotics (such as chronic toxicity, endocrine disorders, etc.) may pose to humans and other living organisms [55]. The present study was aimed to prepare  $\text{Fe}_3\text{O}_4@\text{Cb}$  adsorbent as a new magnetic nanocomposite for removing TC from aqueous media and optimizing the parameters affecting the removal process using the RSM based on CCD.

## 2. Materials and methods

### 2.1. Required chemicals and equipments

In this study, TC powder (purity of 98%) was purchased from Sigma-Aldrich Company, the chemical structure of which is shown in Fig. 1. Other materials including ammonia, hydrochloric acid (HCl), sodium hydroxide (NaOH), methanol, iron(III) chloridehexahydrate, and iron(II) chloridetetrahydrate were purchased from the German Merck Company. The Cb was collected from the Persian Gulf shores. The microstructure, morphology, and chemical composition of  $\text{Fe}_3\text{O}_4@\text{Cb}$  were investigated by field emission scanning electron microscopy (FESEM; MIRA3TESCANXMU). The energy-dispersive X-ray spectroscopy (EDS; MIRA3TESCANXMU) was applied to further confirm the composition and distribution of the elements. Fourier transform infrared (FTIR) spectroscopy (Affinity-1, Shimadzu, Japan) has been used to investigate chemical bonds and adsorbent functional groups in the range 400–4,000  $\text{cm}^{-1}$ . The X-ray diffraction (XRD; X'Pert Pro MPD, Panalytical, Holland) was used to study the crystal structure, grain size, existing phases, and the interaction between them in the adsorbent. The magnetic properties of  $\text{Fe}_3\text{O}_4@\text{Cb}$  were determined by vibrating-sample magnetometer (VSM; Lake Shore Cryotronic-7404) at room temperature. The surface areas of the adsorbent based on nitrogen desorption/adsorption isotherms were evaluated using Brunauer-Emmett-Teller (BET) by a specific surface analyzer (BELSORP-mini II) at 120°C. A shaking device (THZ-98A model, Shanghai, China) was used to shake materials. The adsorbent was separated from the samples by a neodymium magnet. The pH meter (Metrohm 827, Switzerland) was used to read the pH. The residual concentration of TC was determined by high performance liquid

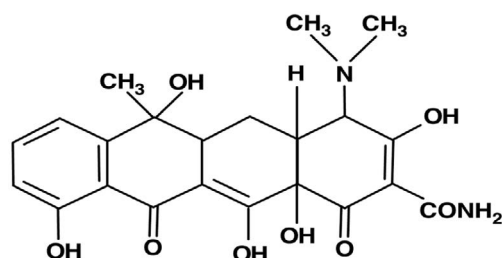


Fig. 1. Chemical structure of TC antibiotic.

chromatography (HPLC; ACC 3000 HPLC) and VWD-3400Rs detector (UV-Visible) at a wavelength of 357 nm. A column of C18 (5  $\mu$ m; 4.6  $\times$  150 mm) was used.

## 2.2. Adsorbent synthesis

The Fe<sub>3</sub>O<sub>4</sub>@Cb magnetic nanocomposite was synthesized by co-precipitation using iron chloride under alkaline conditions. Cb was used after initial preparation such as washing, crushing, and pulverization. For this purpose, Cb powder was washed with deionized distilled water and then boiled for 10 min. It was placed at 100°C for 24 h to desorb all impurities. To synthesize Fe<sub>3</sub>O<sub>4</sub>@Cb magnetic nanocomposite, 0.5 g of Cb powder, 4.5 g of FeCl<sub>3</sub>·6H<sub>2</sub>O, and 2 g of FeCl<sub>2</sub>·4H<sub>2</sub>O were first added to 100 mL of deionized distilled water at 60°C. Next, ammonia was added drop wise to the reaction vessel to complete the reaction under alkaline conditions. Finally, a black powder formed at the bottom of the reaction vessel was separated by a magnet and was washed several times with deionized water to be neutralized. The adsorbent was dried in an oven at 70°C for 24 h.

## 2.3. Design of experiments

Design-Expert 11 software was used based on CCD to design the experiments. In this study, four factors, including adsorbent dosage, pH, contact time, and initial TC concentration were considered as variables and the experiments (run = 30) were designed. The selected levels and code related to the variables used in this study to design the experiments are shown in Table 1.

## 2.4. Experiments

All experiments were performed in a batch reactor with a 250 mL volumetric flask. Based on the obtained runs ( $n = 30$ ) by Design-Expert 11 software, the adsorbent dosage

(0.05–0.25 g/L), pH (3–11), contact time (15–115 min), and initial concentration of TC (4–20 mg/L) were set in each run. Each run was repeated three times to increase the accuracy. The concentration of residual TC in the solution was finally read by HPLC. The removal efficiency of TC obtained in the laboratory (percentage of actual removal efficiency) was recorded in the response column in Design-Expert 11 software and the analysis was performed by the software. Research data were analyzed by multiple regressions, and coefficients were analyzed using the analysis of variance (ANOVA) by considering  $p \leq 0.05$  statistically significant. Finally, two-dimensional diagrams (response surface curves) were plotted to investigate the relationship between response and independent variables.

The removal efficiency of TC was obtained using the following formula [56]:

$$R(\%) = \frac{(C_0 - C_f)}{C_0} \times 100 \quad (1)$$

where  $R$  is the removal efficiency of TC (%),  $C_0$  is the initial concentration of TC in aqueous solution (mg/L),  $C_f$  is the final concentration of TC in aqueous solution (mg/L).

Also, the adsorbent adsorption capacity was calculated by the following formula [56]:

$$q_e (\text{mg/g}) = \frac{(C_0 - C_f)V}{M} \quad (2)$$

In this formula,  $q_e$  is the adsorption capacity of the adsorbent (mg/g),  $C_0$  is the initial concentration of TC (mg/L),  $C_f$  is the final concentration of TC (mg/L),  $V$  is the volume of solution (L), and  $M$  is the amount of adsorbent used (g).

The hospital wastewater was used to evaluate the efficiency of Fe<sub>3</sub>O<sub>4</sub>@Cb magnetic nanocomposite in removing TC from the real sample. The real sample was collected from the wastewater of one of the hospitals in Kerman, Iran, and after adding a certain amount of TC, its physicochemical characteristics were determined. Experiments were performed on the wastewater under optimum conditions and the removal efficiency of TC by the Fe<sub>3</sub>O<sub>4</sub>@Cb magnetic nanocomposite was reported.

## 2.5. Determining $pH_{pzc}$

The  $pH_{pzc}$  ( $pH_{\text{point of zero charge}}$ ) of the adsorbent was determined as follows: first, 50 mL of 0.1 M sodium chloride solution was poured into eleven 100 mL Erlenmeyer flasks. The initial pH was adjusted in all Erlenmeyer flasks by

Table 1  
Selected levels and code related to the variables used in this study to design the experiments

Factor	Name	Units	Minimum	Maximum	Coded low	Coded high
A	pH	—	3	11.00	-1 $\leftrightarrow$ 5.00	+1 $\leftrightarrow$ 9.00
B	Initial concentration	mg/L	4	20.00	-1 $\leftrightarrow$ 8.00	+1 $\leftrightarrow$ 16.00
C	Adsorbent dosage	g/L	0.05	0.25	-1 $\leftrightarrow$ 0.1	+1 $\leftrightarrow$ 0.2
D	Contact time	min	15	115.00	-1 $\leftrightarrow$ 40.00	+1 $\leftrightarrow$ 90.00

sodium hydroxide and 1 M hydrochloric acid in the range of 1–11. Then, 0.2 g of  $\text{Fe}_3\text{O}_4@\text{Cb}$  magnetic nanocomposite was added to all Erlenmeyer flasks and the shaking device was set at 120 rpm for 48 h. After 48 h the adsorbent was separated with a neodymium magnet and the pH was measured again in all Erlenmeyer flasks and recorded as the final pH. Finally, the diagram of initial pH versus  $\Delta\text{pH} = \text{final pH} - \text{initial pH}$  was plotted by Excel 2007, and the value of  $\text{pH}_{\text{pzc}}$  was detected when  $\Delta\text{pH}$  was zero [56].

### 3. Results and discussion

#### 3.1. Specifications of $\text{Fe}_3\text{O}_4@\text{Cb}$ magnetic nanocomposite

##### 3.1.1. Vibrating-sample magnetometer

The magnetic properties of  $\text{Fe}_3\text{O}_4@\text{Cb}$  nanocomposite were investigated by VSM at room temperature (Fig. 2). As can be seen in Fig. 2, the value of saturation magnetization ( $M_s$ ) of  $\text{Fe}_3\text{O}_4@\text{Cb}$  nanocomposite was equal to 49.62 emu/g, indicating the ferromagnetic properties of the nanocomposite. This amount of  $M_s$  allows the nanocomposite to be easily separated from the TC solution by a magnet after the adsorption process is complete. Also, collecting the magnetic nanocomposite from wastewater does not require time-consuming and costly methods such as filtration and centrifugation and will not cause secondary pollution in the environment and can be reused for later stages and recycled.

##### 3.1.2. Brunauer-Emmett-Teller

The specific surface area of Brunauer, Emmett, Teller (BET)–Barrett, Joyner, Halenda (BJH) and the adsorption/desorption isotherm of the synthesized  $\text{Fe}_3\text{O}_4@\text{Cb}$  magnetic nanocomposite are shown in Figs. 3a and

b. The specific surface area of the synthesized  $\text{Fe}_3\text{O}_4@\text{Cb}$  magnetic nanocomposite was 89.148  $\text{m}^2/\text{g}$ . The mean pore diameter and total pore volume were 14.427 nm and 0.3215  $\text{cm}^3/\text{g}$ , respectively.  $\text{Fe}_3\text{O}_4@\text{Cb}$  nanocomposite can be classified as a mesoporous material [57].

##### 3.1.3. X-ray diffraction

The XRD pattern of  $\text{Fe}_3\text{O}_4@\text{Cb}$  magnetic nanocomposite showed the ferrite crystalline phase with peaks at  $2\theta$  from 18.41°, 30.29°, 35.68°, 43.36°, 43.36°, 53.81°, 57.36°, 63.00°, 71.49°, and 76.54° (Fig. 4). The sample was consistent with JCPDS code No. 22–1086 and confirmed the ferrite structure of  $\text{Fe}_3\text{O}_4$ . As can be seen in Fig. 4, sharp peaks represent

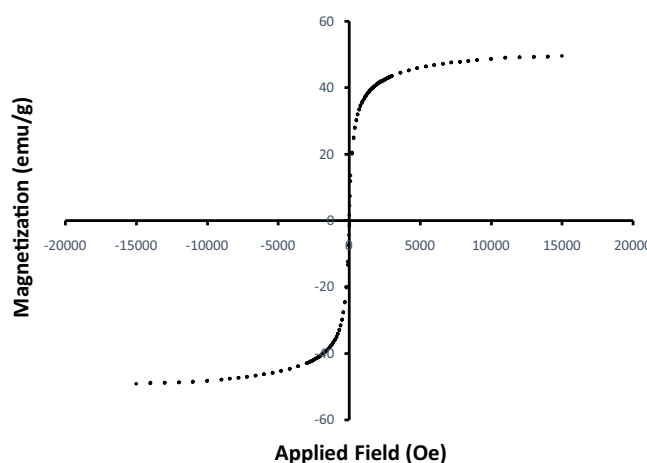


Fig. 2. The VSM magnetization curve of the  $\text{Fe}_3\text{O}_4@\text{Cb}$  magnetic nanocomposite.

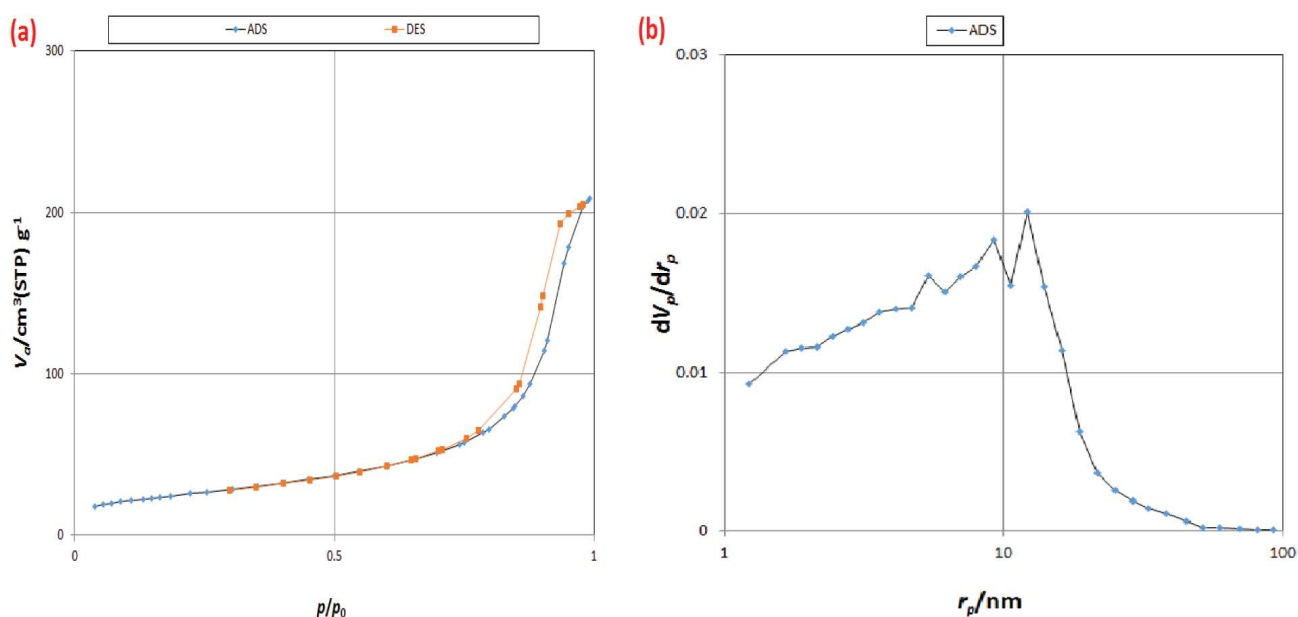


Fig. 3. (a) The nitrogen adsorption/desorption isotherm and (b) the pore size distributions of the  $\text{Fe}_3\text{O}_4@\text{Cb}$  magnetic nanocomposite.

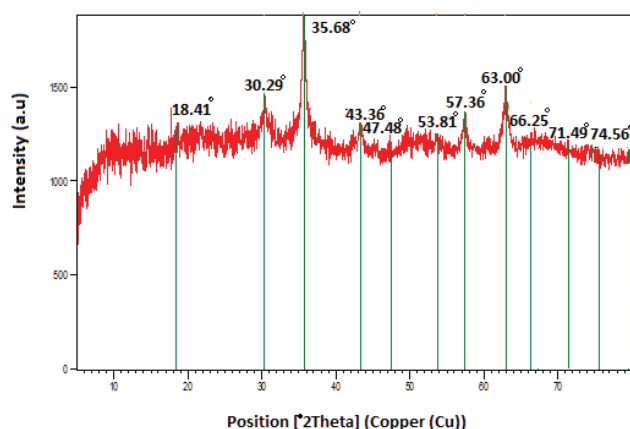


Fig. 4. The XRD analysis of the  $\text{Fe}_3\text{O}_4@\text{Cb}$  magnetic nanocomposite.

the crystalline structure of  $\text{Fe}_3\text{O}_4$ , which has been preserved after compositing with Cb. Also, the peaks observed in  $47.48^\circ$  and  $66.25^\circ$  can be related to Cb.

#### 3.1.4. Field emission scanning electron microscopy

Fig. 5 shows the FESEM image of the  $\text{Fe}_3\text{O}_4@\text{Cb}$  magnetic nanocomposite. According to Fig. 5, FESEM shows the formation of nanoparticles in an average particle size of approximately 31 nm, with the least amount of agglomeration and a uniform quasi-spherical structure.

#### 3.1.5. Mapping

The EDS mapping was used to determine the distribution of the constituent elements of the  $\text{Fe}_3\text{O}_4@\text{Cb}$  magnetic nanocomposite (Figs. 6a–j). According to Figs. 6a–j, the elements of carbon, iron, nitrogen, sodium, calcium,

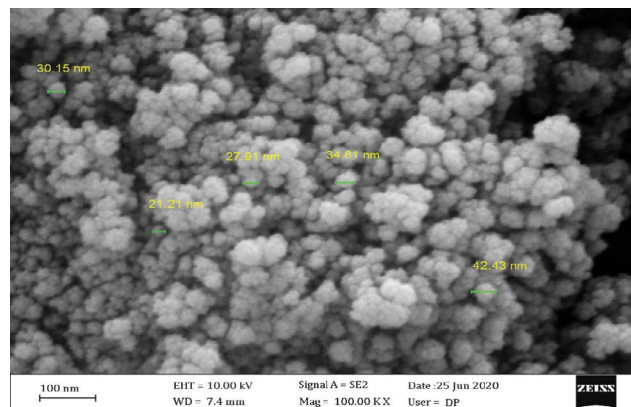


Fig. 5. The FESEM images of the  $\text{Fe}_3\text{O}_4@\text{Cb}$  magnetic nanocomposite.

magnesium, oxygen, phosphorus, and sulfur had a uniform distribution in the structure of the magnetic nanocomposite, indicating the high uniformity of synthesized  $\text{Fe}_3\text{O}_4@\text{Cb}$ .

#### 3.1.6. Energy-dispersive X-ray spectroscopy

EDSs were investigated to evaluate the chemical composition of the  $\text{Fe}_3\text{O}_4@\text{Cb}$  magnetic nanocomposite (Fig. 7). The results showed that 67.1% iron, 27.5% oxygen, 4.7% carbon, 0.3% sodium, 0.2% sulfur, 0.1% calcium, and 0.1% phosphorus were consistent with the predicted values in the chemical structure of the  $\text{Fe}_3\text{O}_4@\text{Cb}$  magnetic nanocomposite.

#### 3.1.7. Fourier transform infrared spectroscopy

The FTIR spectrum of Cb and the  $\text{Fe}_3\text{O}_4@\text{Cb}$  magnetic nanocomposite at  $400\text{--}4,000\text{ cm}^{-1}$  are shown in Figs. 8a and b, respectively.

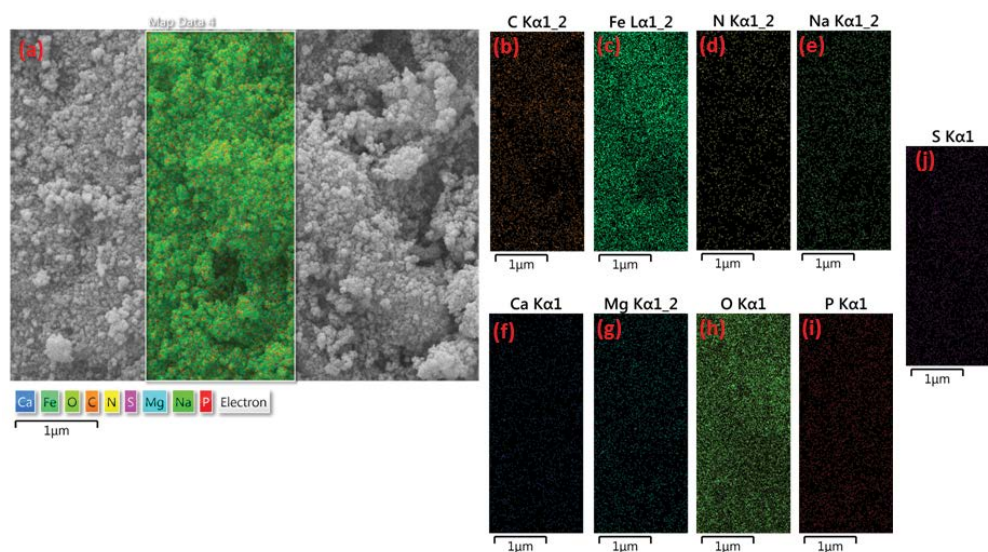


Fig. 6. The elemental mapping images of the as-prepared  $\text{Fe}_3\text{O}_4@\text{Cb}$  magnetic nanocomposite (a) Ca, Fe, O, C, N, S, Mg, Na, and P, (b) carbon, (c) iron, (d) nitrogen, (e) sodium, (f) calcium, (g) magnesium, (h) oxygen, (i) phosphorus, and (j) sulfur.

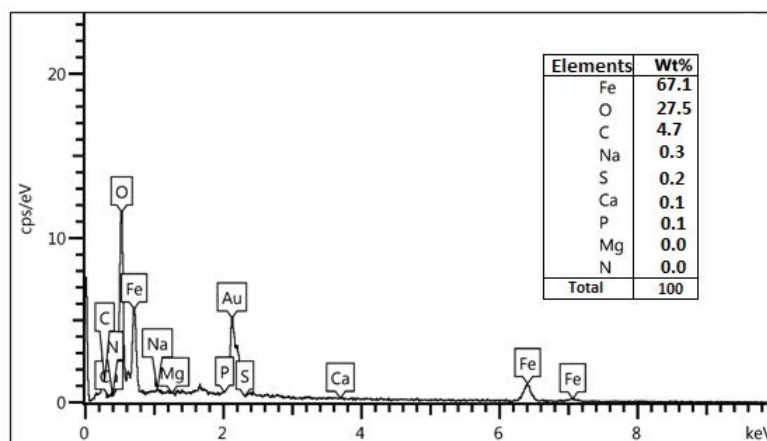


Fig. 7. EDS pattern of the as-prepared  $\text{Fe}_3\text{O}_4@\text{Cb}$  magnetic nanocomposite.

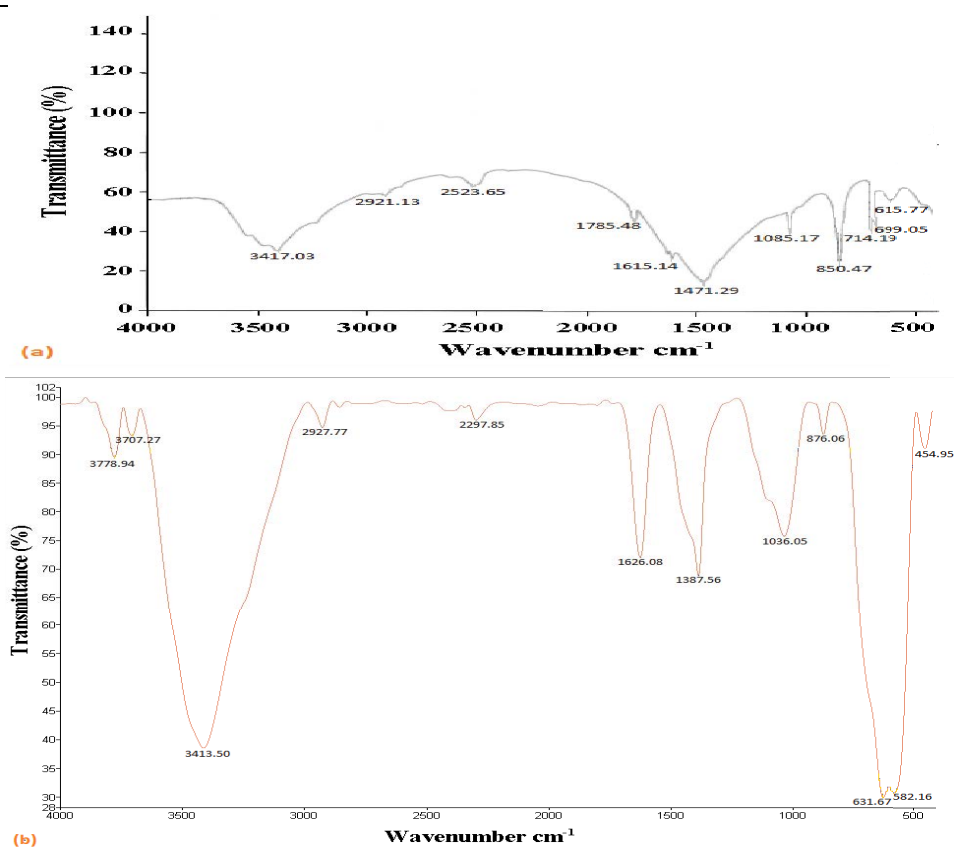


Fig. 8. (a) FTIR of Cb and (b)  $\text{Fe}_3\text{O}_4@\text{Cb}$ .

As shown in Figs. 8a and b, a wide adsorption band is observed in  $3,417.03\text{ cm}^{-1}$ , which can be related to the O–H stretching vibrations of the moisture adsorbed on the adsorbent surface. The presence of the band at  $2,921.13\text{ cm}^{-1}$  is due to the alkyl groups (C–H). The presence of an adsorption band at  $2,523.65\text{ cm}^{-1}$  is due to the amine groups (N–H) in the Cb structure. Adsorption bands at  $1,471.29\text{ cm}^{-1}$  can be related to pyranose ring

bending vibrations. Adsorption bands at  $1,085.17$ ,  $850.47$ , and  $714.19\text{ cm}^{-1}$  correspond to C–O, C–H, and C–H<sub>2</sub> stretching vibrations, respectively [58,59].

### 3.2. Response surface methodology

The number of runs obtained based on the parameters by the software and the actual removal efficiency in the

laboratory as well as the predicted value by the software is shown in Table 2. According to the results presented in Table 2, the maximum of TC removal efficiency was calculated as 80.02% in the run No. 14 and the pH conditions equal to 5, adsorbent dosage of 0.2 g/L, initial concentration of TC of 16 mg/L, and contact time of 90 min. In addition, the adsorption capacity by the adsorbent varied between 1.76 and 14.94 mg/g at different runs, indicating a relatively good adsorption capacity. Fig. 9 also shows the actual values versus the predicted values. Based on the results of Table 2 and Fig. 9, the actual response values are close to the predicted values, indicating the model is suitable.

In addition, Fig. 10 compares the removal efficiency (%) and adsorption capacity (mg/g) of TC from aqueous solution by Fe<sub>3</sub>O<sub>4</sub>@Cb magnetic nanocomposite in 30 laboratory runs. As can be seen, the maximum removal efficiency and adsorption capacity were calculated as 80.02% and 149.44 mg/g in the run Nos. 14 and 17, respectively.

### 3.3. Appropriate model, equation, and ANOVA results

As shown in Table 3, the quadratic model was provided by the software to describe the process. In this model, the value of  $R^2$  is equal to 0.9723; since this number is close to 1, it indicates that the model is suitable. Also, the  $R^2$  value predicted by the model is equal to 0.8525, which has been adjusted in a reasonable agreement with  $R^2$ , the value of which is equal to 0.9465 and their difference is less than 0.2. Adequate precision measures the signal-to-noise ratio. A ratio greater than 4 is desirable. This ratio was 25.141 in our model, indicating a sufficient signal, and this model can be used to guide the design space.

The ANOVA results obtained by the software for the proposed model are shown in Table 4. For the proposed model, the  $F$  value was equal to 37.67, confirming that the model is significant and there is only a 0.01% chance that a large  $F$  value occurs due to noise. Also, the  $p$  value

Table 2

The design of experiments with predicted and laboratory values for the removal of TC by Fe<sub>3</sub>O<sub>4</sub>@Cb magnetic nanocomposite using RSM method based on CCD

Run	A: pH	B: initial concentration (mg/L)	C: adsorbent dosage (g/L)	D: contact time (min)	Removal efficiency (%)		Adsorption capacity (mg/g)
					Actual	Predicted	
1	9	16	0.1	90	68.09	66.85	10.89
2	5	16	0.1	40	71.52	71.11	11.44
3	7	12	0.15	65	69.82	69.81	5.58
4	7	12	0.15	65	70.01	69.81	5.60
5	7	12	0.15	65	70.32	69.81	5.62
6	5	8	0.2	40	70.2	70.17	2.80
7	5	8	0.1	90	71.23	71.48	5.69
8	9	8	0.1	40	60.46	60.67	4.83
9	9	8	0.1	90	65.56	64.79	5.24
10	5	16	0.2	40	74.23	75.35	5.93
11	7	12	0.15	65	69.95	69.81	5.59
12	9	8	0.2	90	71.04	70.18	2.84
13	5	16	0.1	90	74.84	75.22	11.97
14	5	16	0.2	90	80.02	78.54	6.40
15	11	12	0.15	65	63.38	64.46	5.07
16	7	12	0.15	115	74.56	75.25	5.96
17	7	12	0.05	65	62.27	62.96	14.94
18	7	20	0.15	65	73.17	73.73	9.75
19	7	4	0.15	65	66.13	66.50	1.76
20	9	8	0.2	40	67	66.97	2.68
21	3	12	0.15	65	76.19	76.03	6.09
22	9	16	0.2	90	72.69	73.79	5.81
23	9	16	0.2	40	71.99	70.47	5.75
24	5	8	0.1	40	68.25	67.50	5.46
25	7	12	0.15	15	67.72	67.95	5.41
26	7	12	0.15	65	68.75	69.81	5.58
27	7	12	0.15	65	70.03	69.81	5.60
28	9	16	0.1	40	62.58	62.61	10.01
29	7	12	0.25	65	72.36	72.59	1.87
30	5	8	0.2	90	72.92	73.24	2.91

obtained less than 0.05, indicating that the model is statistically significant. In this case, *A*, *B*, *C*, *D*, *AC*, *C*<sup>2</sup>, and *D*<sup>2</sup> are significant model terms. Values greater than 0.1 indicate that the model terms are not significant. The lack of fit *F* value of the model was 4.58, which was greater than 0.05, confirming that the lack of fit is not statistically significant and there is only a 5.35% chance that a large lack of fit *F* value occurs due to noise. The insignificant lack of fit is a good indication that our model is appropriate.

The final equation (Eq. (3)) with coded term factors for the quadratic model provided by the software was as follows:

$$\text{Removal efficiency} = +69.81 - 2.89A + 1.81B + 2.41C + 1.83D - 0.4200AB + 0.9063AC + 0.0338AD + 0.3900BC + 0.0300BD - 0.2287CD + 0.1081A^2 + 0.0744B^2 - 0.5094C^2 + 0.4469D^2 \quad (3)$$

The equation with coded term factors can be used to predict the response for certain levels of each factor. By default, the high levels of the factors are coded as +1 and the low levels are coded as -1. The coded equation is useful for identifying the relative effect of factors by comparing factor coefficients. Also, the actual equation (Eq. (4)) for the quadratic model provided by the software was as follows:

$$\begin{aligned} \text{Removal efficiency} = & +70.35066 - 2.59794 \text{ pH} + 0.395812 \\ & \text{initial concentration} + 3.42992 \text{ adsorbent dosage} - \\ & 0.000758 \text{ contact time} - 0.052500 \text{ pH} \times \text{initial concentration} \\ & + 0.906250 \text{ pH} \times \text{adsorbent dosage} + 0.000675 \\ & \text{pH} \times \text{contact time} + 0.195000 \text{ initial concentration} \times \\ & \text{adsorbent dosage} + 0.000300 \text{ initial concentration} \times \\ & \text{contact time} - 0.018300 \text{ adsorbent dosage} \times \\ & \text{contact time} + 0.027031 \text{ pH}^2 + 0.004648 \\ & \text{initial concentration}^2 - 2.03750 \text{ adsorbent dosage}^2 + \\ & 0.000715 \text{ contact time}^2 \end{aligned} \quad (4)$$

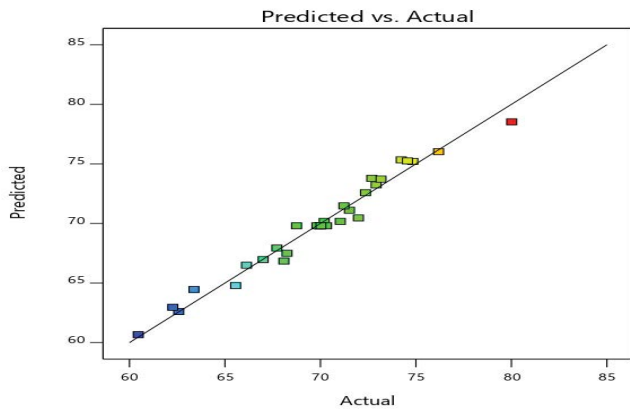


Fig. 9. Diagram of laboratory (actual) values versus the predicted values provided by Design-Expert 11 software.

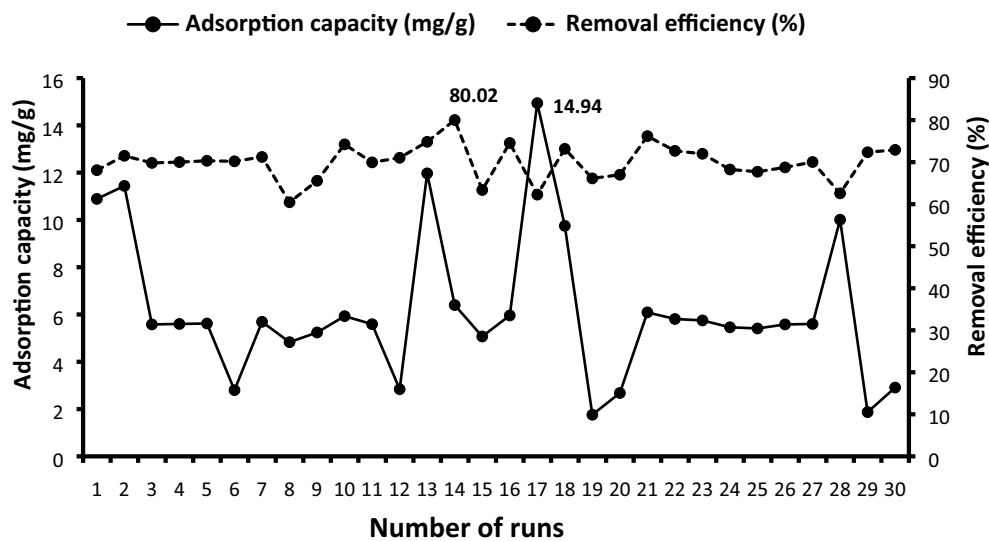


Fig. 10. Comparison of removal efficiency (%) and adsorption capacity (mg/g) of TC from a synthetic aqueous solution by Fe<sub>3</sub>O<sub>4</sub>@Cb magnetic nanocomposite in 30 laboratory runs.

Table 3  
The model proposed by the software; predicted *R*<sup>2</sup> and adjusted *R*<sup>2</sup> values

Source	Sequential <i>p</i> value	Lack of fit <i>p</i> value	<i>R</i> <sup>2</sup>	Adjusted <i>R</i> <sup>2</sup>	Predicted <i>R</i> <sup>2</sup>	Adequate precision	
Quadratic	<0.0001	0.0535	0.9723	0.9465	0.8525	25.141	Suggested

Table 4

The ANOVA results of the proposed model for the removal of TC antibiotic from aqueous solution by  $\text{Fe}_3\text{O}_4@\text{Cb}$  magnetic nanocomposite using RSM method based on CCD

Source	Sum of squares	Df	Mean square	F value	p value	
Model	532.67	14	38.05	37.67	<0.0001	Significant
A: pH	200.80	1	200.80	198.83	<0.0001	
B: initial concentration	78.41	1	78.41	77.64	<0.0001	
C: adsorbent dosage	138.91	1	138.91	137.55	<0.0001	
D: contact time	80.08	1	80.08	79.30	<0.0001	
AB	2.82	1	2.82	2.79	0.1153	
AC	13.14	1	13.14	13.01	0.0026	
AD	0.0182	1	0.0182	0.0180	0.8949	
BC	2.43	1	2.43	2.41	0.1414	
BD	0.0144	1	0.0144	0.0143	0.9065	
CD	0.8372	1	0.8372	0.8290	0.3770	
A <sup>2</sup>	0.3207	1	0.3207	0.3175	0.5814	
B <sup>2</sup>	0.1517	1	0.1517	0.1502	0.7038	
C <sup>2</sup>	7.12	1	7.12	7.05	0.0180	
D <sup>2</sup>	5.48	1	5.48	5.42	0.0343	
Residual	15.15	15	1.01			
Lack of fit	13.66	10	1.37	4.58	0.0535	Not significant
Pure error	1.49	5	0.2983			
Corrected total	547.81	29				

The equation with actual term factors can be used to predict the response for certain levels of each factor. Here, the levels should be specified for each factor in the main units. This equation should not be used to determine the relative effect of each factor, because the coefficients are scaled to match the units of each factor and the  $y$ -intercept is not at the center of the design space.

### 3.4. Surface response diagrams

Based on the results shown in Table 2 and Figs. 12 and 13a–c, in general, with increasing initial concentration, adsorbent dosage, and contact time, the removal efficiency of TC from aqueous solution using  $\text{Fe}_3\text{O}_4@\text{Cb}$  magnetic nanocomposite increased. However, with increasing pH, the removal efficiency of TC decreased.

The removal of antibiotics from aqueous solution depends largely on the pH of the solution, which affects the surface properties of the nano-adsorbent and the degree of ionization [60]. The effect of pH on the removal efficiency of TC from aqueous solution in the range of 3–11 was examined. Based on the results presented in Table 2 and Figs. 12a–c, at different runs, the removal efficiency of TC at pH 3, 5, 7, 9, and 11 was 76.19%, 68.25%–80.02%, 62.27%–74.56%, 60.46%–72.69%, and 63.38%, respectively. TC varies at different sites depending on the pH of the precipitation solution. When the pH is less than 4, TC becomes cationic ( $\text{TCH}^+$ ) due to the protonation of the dimethyl ammonium group. At pH of 3.5–7.5, TC becomes zwitterion ( $\text{TCH}^0$ ) due to the loss of a proton from the phenolic di-ketone moiety. At pH greater than 7, TC becomes anionic ( $\text{TCH}^-$  or  $\text{TC}^{2-}$ ) due to the loss of protons from the phenolic di-ketone moiety

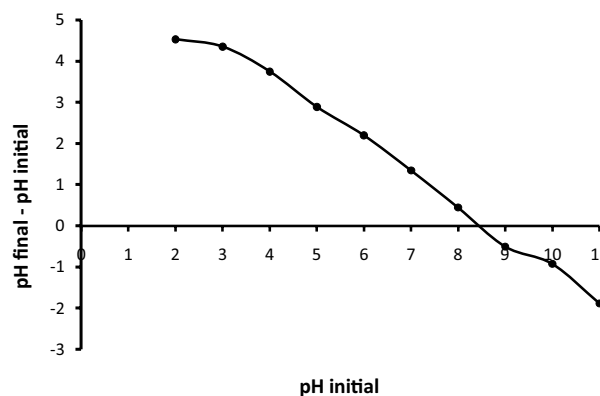


Fig. 11. Determining  $\text{pH}_{\text{pzc}}$  (initial pH versus final pH minus initial pH).

and the tricarbonyl system [60]. The results of this study showed that the removal efficiency of TC from aqueous solution decreased with increasing pH, hence, the cation exchange mechanism of TC adsorption onto the  $\text{Fe}_3\text{O}_4@\text{Cb}$  magnetic nanocomposite was predominant. The adsorption capacity of adsorbent and nature of binding sites are determined with the help of significant factor, which is a point of zero charge ( $\text{pH}_{\text{pzc}}$ ) [35]. Based on the results obtained in Fig. 11, the value of  $\text{pH}_{\text{pzc}}$  for the  $\text{Fe}_3\text{O}_4@\text{Cb}$  magnetic nanocomposite was equal to 8.5, i.e., at  $\text{pH} < 8.5$ , the nanocomposite surface charge is positive and at  $\text{pH} > 8.5$ , the nanocomposite surface charge is negative. It is always easy to adsorb a cation on a negatively charged surface and an anion on a positively charged surface. However, other interactions

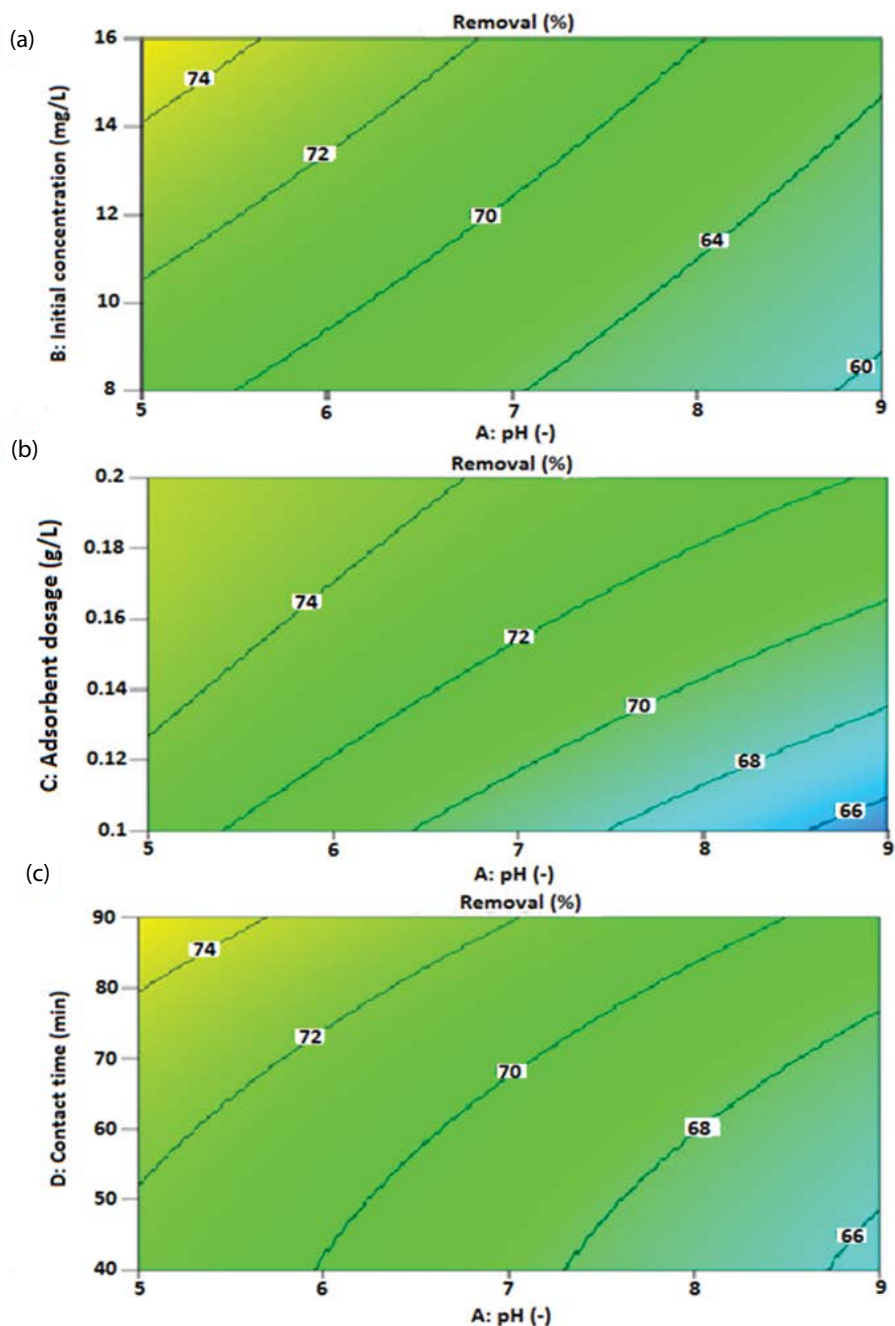


Fig. 12. (a) The contour plot of the removal efficiency of TC from aqueous solution by  $\text{Fe}_3\text{O}_4@\text{Cb}$  magnetic nanocomposite in terms of pH and initial concentration at the central constant level of contact time and adsorbent dosage. (b) The contour plot of the removal efficiency of TC from aqueous solution by  $\text{Fe}_3\text{O}_4@\text{Cb}$  magnetic nanocomposite in terms of pH and adsorbent dosage at the central constant level of contact time and initial concentration. (c) The contour plot of the removal efficiency of TC from aqueous solution by  $\text{Fe}_3\text{O}_4@\text{Cb}$  magnetic nanocomposite in terms of pH and contact time at the central constant level of adsorbent dosage and initial concentration.

may be stronger than just electrostatic forces, which make the surface charge effect less important. In addition, a cation is often complexed with ligands, some of which may be negatively charged. Therefore, in this case, the cation is actually a negative complex that may very well adsorb on the positive surface, which is what happened in this study. It can be said that the adsorption mechanism at  $2 < \text{pH} < 3$

was as cation exchange. At  $3 < \text{pH} < 7$ , the adsorption mechanism was in the form of cation exchange and surface complexation, and at  $\text{pH} < 7$ , the adsorption mechanism was in the form of surface complexation. Besides, adsorption of TC on the  $\text{Fe}_3\text{O}_4@\text{Cb}$  magnetic nanocomposite depends on the specific area; number of functional groups which may lead to electrostatic, hydrophobic, and hydrogen bonding;

ability to form host–guest complexes; and charge transfer that all these interactions can be affected by the change of pH [61]. In their study, Maryoosh et al. [62] used cobalt oxide to remove TC antibiotic from the aqueous solution and found that the removal efficiency of TC decreased with increasing pH. Also, Mohammed and Kareem [63] employed pistachio shell coated with ZnO nanoparticles to remove TC antibiotics from aqueous solutions and found that the removal efficiency of TC decreased as pH value increased and the maximum removal efficiency was obtained at pH 5. The results of our study are not consistent with the results of Foroughi et al.'s study [61] on the use of Fe<sub>3</sub>O<sub>4</sub>-g-CN@PEI-β-CD nanocomposite and the study of Yang et al. [64] on the use of magnetic carbon-coated cobalt oxide nanoparticles to remove TC from aqueous solutions.

The initial concentration of TC is another parameter affecting the adsorption process, which was examined in the range of 4–20 mg/L in our study. Based on the results presented in Table 2 and Figs. 12a and 13a & b, at different runs, the removal efficiency of TC from aqueous solution in initial TC concentrations of 4, 8, 12, 16, and 20 mg/L was 66.13%, 60.46%–72.92%, 62.27%–76.19%, 62.58%–80.02%, and 73.17%, respectively. In general, with increasing the initial concentration of TC, the removal efficiency of TC from aqueous solution increased. This may be due to an increase in the driving force applied to the nano-adsorbent with an increase in the initial TC concentration. In their study, Mohammed and Kareem [63] used pistachio shell coated with ZnO nanoparticles as an adsorbent to remove TC from aqueous solutions. They found that the removal efficiency of TC increased from 72.06% to 84.87% as the initial concentration of TC increased from 30 to 70 ppm. However, in Foroughi et al.'s [61] study on the use of Fe<sub>3</sub>O<sub>4</sub>-g-CN@PEI-β-CD nanocomposite and in the study of Maryoosh et al. [62] on the use of cobalt oxide adsorbent to remove TC from aqueous solutions, the removal efficiency of TC decreased by increasing the initial TC concentration. These studies [61,62] stated that the reason could be attributed to the restriction of the adsorption process at a high antibiotic loading level caused by the limited number of effective adsorption sites.

Adsorbent dosage is another important parameter that can affect the adsorption capacity of TC by nanocomposites. The removal efficiency of TC from aqueous solution was investigated in the adsorbent dosage of 0.05–0.25 g/L. Based on the results presented in Table 2 and Figs. 12b and 13a & c, at different runs, the removal efficiency of TC from aqueous solution at adsorbent dosages of 0.05, 0.1, 0.15, 0.2, and 0.25 was equal to 62.27%, 60.46%–74.84%, 63.38%–76.19%, 67%–80.02%, and 72.36%, respectively. In general, the removal efficiency of TC from aqueous solution increased with increasing adsorbent dosage. As the adsorbent dosage increases, the number of active sites also increases, hence, a larger surface area is provided for adsorption. Therefore, a greater number of molecules of the adsorbent are absorbed, which leads to further removal of the antibiotic. A possible explanation for this phenomenon is that with the increasing concentration of the adsorbent, more active sites are available for TC; this will effectively abate the competition for a certain adsorption site and thus enhance the adsorption capacity [65]. In their study, Bangari and Sinha [24]

used boron nitride nanosheets as an adsorbent to remove TC from aqueous solution, and found that the removal efficiency of TC increased from 55% to 85% as the adsorbent dosage increased from 0.2 to 1 g/L. Also, Mohammed and Kareem [63] employed ZnO nanoparticles as adsorbents to remove TC from wastewater, and reported that the removal efficiency of TC increased from 61.73% to 85.29% by increasing the adsorbent dosage from 0.02 to 0.08 g/L.

Contact time is one of the most important factors in evaluating the efficiency of the adsorbent [63]. The effect of contact time in the range of 15–115 min on the removal efficiency of TC from aqueous solution was examined. Based on the results presented in Table 2 and Figs. 12c and 13b & c, the removal efficiency of TC from aqueous solution increased with increasing contact time and then reached an equilibrium state, so that at different runs, the removal efficiency of TC after 15, 40, 65, 90, and 115 min was equal to 67.72%, 60.46%–74.23%, 62.27%–76.19%, 65.56%–80.02%, and 74.56%, respectively. At the beginning of adsorption, the numerous pores and structural groups on the nanocomposite provided sufficient adsorption, so that TC ions/molecules easily adhere to the nanocomposite. When adsorption occurs, the availability of effective adsorption sites gradually decreases and the adsorption rate slows down until it reaches the equilibrium state. As a result, the remaining vacant surface sites are difficult to be occupied due to the formation of repulsive forces between the TC molecules on the solid surface and in the bulk phase [66]. Guler and Sarioglu [67] used pumice stone as an adsorbent to remove TC from wastewater and found that the removal efficiency of TC increased from 40% to 75% by increasing the contact time from 20 to 120 min. Also, Zhao et al. [68] used KOH-derived from reed plants activated biochar as an adsorbent to remove TC from aqueous solution and reported that the removal efficiency of TC increased with increasing contact time and then reached equilibrium.

### 3.5. Optimization

One of the important aims of this study was to find the optimum process parameters to increase the response using the proposed mathematical model. According to the results shown in Table 5, the pH of 5, initial TC concentration of 8 mg/L, adsorbent dosage of 0.2 g/L, and the contact time of 90 min, with removal efficiency of 73.24% were presented as optimum conditions by the software. The optimum conditions provided by the software were evaluated and compared with real and synthetic wastewater samples in laboratory conditions. As can be seen in Table 5, the removal efficiency of TC in real and synthetic wastewater samples was 75.34% and 80.15%, respectively. It can be observed that the TC removal efficiency in laboratory and synthetic conditions is close to the rate of TC removal efficiency predicted by the software.

### 3.6. Comparison of the performance of Fe<sub>3</sub>O<sub>4</sub>@Cb magnetic nanocomposite with Cb adsorbent

In Fig. 14, the removal efficiency of TC antibiotic from aqueous solution by Fe<sub>3</sub>O<sub>4</sub>@Cb magnetic nanocomposite is compared with Cb adsorbent. As can be seen, the removal

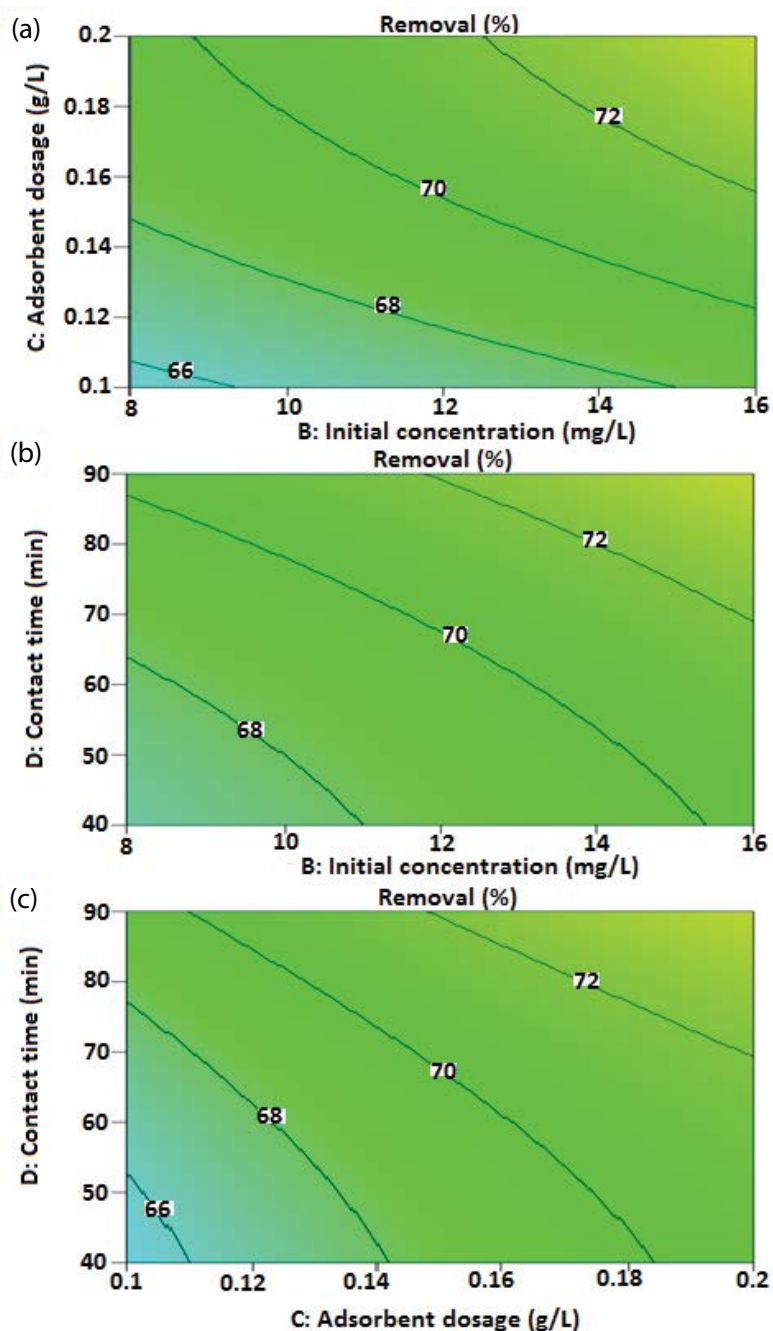


Fig. 13. (a) The contour plot of the removal efficiency of TC from aqueous solution by  $\text{Fe}_3\text{O}_4@\text{Cb}$  magnetic nanocomposite in terms of initial concentration and adsorbent dosage at the central constant level of pH and contact time. (b) The contour plot of the removal efficiency of TC from aqueous solution by  $\text{Fe}_3\text{O}_4@\text{Cb}$  magnetic nanocomposite in terms of initial concentration and contact time at the central constant level of pH and adsorbent dosage. (c) The contour plot of the removal efficiency of TC from aqueous solution by  $\text{Fe}_3\text{O}_4@\text{Cb}$  magnetic nanocomposite in terms of adsorbent dosage and contact time at the central constant level of pH and initial concentration.

efficiency of TC by Cb adsorbent was 36.5% after 90 min, while the removal efficiency of TC by  $\text{Fe}_3\text{O}_4@\text{Cb}$  magnetic nanocomposite reached 79.23% after 90 min, i.e., it increased by 42.73%. Therefore, it can be concluded that magnetization of Cb adsorbent has a positive effect on the removal efficiency of TC and improves its adsorption properties.

### 3.7. Comparison of the performance of $\text{Fe}_3\text{O}_4@\text{Cb}$ magnetic nanocomposite with other adsorbents

Table 6 compares the maximum adsorption capacity of  $\text{Fe}_3\text{O}_4@\text{Cb}$  magnetic nanocomposite for the removal of TC antibiotic with other adsorbents. As can be seen, the adsorption capacity of the  $\text{Fe}_3\text{O}_4@\text{Cb}$  magnetic nanocomposite for

Table 5

Optimum values predicted by the software with the TC removal efficiency under optimum conditions in real and synthetic wastewater samples

	pH	Initial concentration (mg/L)	Adsorbent dosage (g/L)	Contact time (min)	Removal efficiency (%)
Predicted by software	5	8	0.2	90	73.24
Synthetic sample	5	8	0.2	90	80.15
Wastewater actual sample	5	7	0.2	90	75.34

Table 6

Comparison of the maximum adsorption capacity of  $\text{Fe}_3\text{O}_4@\text{Cb}$  magnetic nanocomposite for the removal of TC with adsorbents investigated in other studies

Adsorbent type	Adsorption capacity $q_{\text{max}}$ (mg/g)	Reference
BR-MIL-53 (Fe)	309.6	[47]
Iron loaded sludge biochar	104.86	[69]
Biochar derived from waste <i>Auricularia auricula</i> dregs	11.9	[70]
Magnetic carbon-coated cobalt oxide nanoparticles	769.43	[64]
Raw olive solid wastes	16	[71]
Olive solid wastes/chitosan composite	1.6	[71]
Cobalt-impregnated spent coffee ground biochar	370.37	[72]
Wasted sludge-based biochar modified by chitosan and Fe/S	183.01	[73]
Boron nitride nanosheets	346.66	[24]
Magnetic carbon- $\alpha\text{Fe}/\text{Fe}_3\text{C}$	511.06	[74]
Graphene oxide	313	[75]
Nanocomposite multi-walled carbon nanotube functionalized MIL-53 (Fe)	368.49	[76]
Magnetic graphene oxide sponge	473	[44]
$\text{Fe}_3\text{O}_4\text{-g-CN@PEI-}\beta\text{-CD}$ nanocomposite	833.33	[61]
$\text{Fe}_3\text{O}_4@\text{Cuttlebone}$	14.94	This study

removing TC is better than a number of other adsorbents, which can be attributed to its nanostructure and surface properties.

#### 4. Conclusion

In this study, the removal efficiency of TC antibiotic from aqueous solution by the new  $\text{Fe}_3\text{O}_4@\text{Cb}$  magnetic nanocomposite was investigated and the parameters affecting the removal process were optimized using the RSM based on CCD. The nanocomposite structural characterization was investigated using FTIR, FESEM, EDS, mapping, XRD, BET, and VSM techniques. The quadratic model was suggested as the best model for the removal of TC using the  $\text{Fe}_3\text{O}_4@\text{Cb}$  magnetic nanocomposite. The  $R^2$  value of the model for the removal of TC from aqueous solution was 0.9723. The  $\text{Fe}_3\text{O}_4@\text{Cb}$  magnetic nanocomposite was synthesized at the nanometer scale (approximately 31 nm). The  $S_{\text{BET}}$  surface area of nanocomposite was  $89.148 \text{ m}^2/\text{g}$ . The maximum removal efficiency of TC by  $\text{Fe}_3\text{O}_4@\text{Cb}$  magnetic nanocomposite could reach 80.02%. Under optimum conditions, the removal efficiency of TC from real wastewater

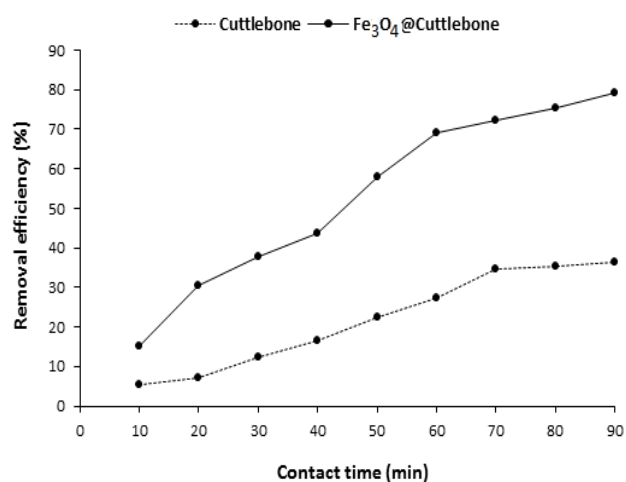


Fig. 14. Comparison of the removal efficiency of TC antibiotic from aqueous solution by  $\text{Fe}_3\text{O}_4@\text{Cb}$  magnetic nanocomposite with Cb adsorbent at pH 5, initial TC concentration of 8 mg/L, adsorbent dosage of 0.2 g/L, and contact time of 90 min.

using Fe<sub>3</sub>O<sub>4</sub>@Cb magnetic nanocomposite was 75.34%. According to the results, Fe<sub>3</sub>O<sub>4</sub>@Cb magnetic nanocomposite can have an effective potential in removing TC antibiotics from synthetic aqueous solution and real wastewater.

### Acknowledgments

This paper was the result of a research project approved by the Student Research Committee of Kerman University of Medical Sciences with No. 98000907 (Ethics ID: IR.KMU.REC.1399.359), which was carried out by the financial support of the Vice-Chancellor for Research and Technology of this university. We would like to thank the Student Research Committee and Environmental Health Engineering Research Center of Kerman University of Medical Sciences for their financial and scientific support.

### References

- J. Jin, Z. Yang, W. Xiong, Y. Zhou, R. Xu, Y. Zhang, J. Cao, X. Li, C. Zhou, Cu and Co nanoparticles co-doped MIL-101 as a novel adsorbent for efficient removal of tetracycline from aqueous solutions, *Sci. Total Environ.*, 650 (2019) 408–418.
- M. Malakootian, H. Mahdizadeh, A. Dehdarirad, M. Amiri Gharaghani, Photocatalytic ozonation degradation of ciprofloxacin using ZnO nanoparticles immobilized on the surface of stones, *J. Dispersion Sci. Technol.*, 40 (2019) 846–854.
- R. Li, Y. Zhang, C.C. Lee, L. Liu, Y. Huang, Hydrophilic interaction chromatography separation mechanisms of tetracyclines on amino-bonded silica column, *J. Sep. Sci.*, 34 (2011) 1508–1516.
- A. Önal, Overview on liquid chromatographic analysis of tetracycline residues in food matrices, *Food Chem.*, 127 (2011) 197–203.
- R. Daghrir, P. Drogui, Tetracycline antibiotics in the environment: a review, *Environ. Chem. Lett.*, 11 (2013) 209–227.
- F. Hernández, J.V. Sancho, M. Ibáñez, C. Guerrero, Antibiotic residue determination in environmental waters by LC-MS, *TrAC, Trends Anal. Chem.*, 26 (2007) 466–485.
- J.J. López-Peñalver, M. Sánchez-Polo, C.V. Gómez-Pacheco, J. Rivera-Utrilla, Photodegradation of tetracyclines in aqueous solution by using UV and UV/H<sub>2</sub>O<sub>2</sub> oxidation processes, *J. Chem. Technol. Biotechnol.*, 85 (2010) 1325–1333.
- V. Andreu, P. Vazquez-Roig, C. Blasco, Y. Picó, Determination of tetracycline residues in soil by pressurized liquid extraction and liquid chromatography tandem mass spectrometry, *Anal. Bioanal. Chem.*, 394 (2009) 1329–1339.
- F. Liu, G.-G. Ying, R. Tao, J.-L. Zhao, J.-F. Yang, L.-F. Zhao, Effects of six selected antibiotics on plant growth and soil microbial and enzymatic activities, *Environ. Pollut.*, 157 (2009) 1636–1642.
- A.L. Spongberg, J.D. Witter, Pharmaceutical compounds in the wastewater process stream in Northwest Ohio, *Sci. Total Environ.*, 397 (2008) 148–157.
- J. Gomes, R. Costa, R.M. Quinta-Ferreira, R.C. Martins, Application of ozonation for pharmaceuticals and personal care products removal from water, *Sci. Total Environ.*, 586 (2017) 265–283.
- W. Yang, Y. Wu, L. Zhang, J. Jiang, L. Feng, Removal of five selected pharmaceuticals by coagulation in the presence of dissolved humic acids and kaolin, *Desal. Water Treat.*, 54 (2015) 1134–1140.
- E. Hapeshi, A. Achilleos, M.I. Vasquez, C. Michael, N.P. Xekoukoulotakis, D. Mantzavinos, D. Kassinos, Drugs degrading photocatalytically: kinetics and mechanisms of ofloxacin and atenolol removal on titania suspensions, *Water Res.*, 44 (2010) 1737–1746.
- M. Malakootian, M. Khatami, H. Mahdizadeh, A. Nasiri, M. Amiri Gharaghani, A study on the photocatalytic degradation of p-Nitroaniline on glass plates by thermo-immobilized ZnO nanoparticle, *Inorg. Nano-Metal Chem.*, 50 (2020) 124–135.
- M. Malakootiana, A. Nasiria, A.N. Alibeigic, H. Mahdizadehb, M.A. Gharaghani, Synthesis and stabilization of ZnO nanoparticles on a glass plate to study the removal efficiency of acid red 18 by hybrid advanced oxidation process (ultraviolet/ZnO/ultrasonic), *Desal. Water Treat.*, 170 (2019) 325–336.
- M. Malakootian, A. Nasiri, M. Amiri Gharaghani, Photocatalytic degradation of ciprofloxacin antibiotic by TiO<sub>2</sub> nanoparticles immobilized on a glass plate, *Chem. Eng. Commun.*, 207 (2020) 56–72.
- M. Malakootian, A. Nasiri, A. Asadipour, M. Faraji, E. Kargar, A facile and green method for synthesis of ZnFe<sub>2</sub>O<sub>4</sub>@CMC as a new magnetic nanophotocatalyst for ciprofloxacin removal from aqueous media, *MethodsX*, 6 (2019) 1575–1580.
- M. Malakootian, A. Nasiri, A. Asadipour, E. Kargar, Facile and green synthesis of ZnFe<sub>2</sub>O<sub>4</sub>@CMC as a new magnetic nanophotocatalyst for ciprofloxacin degradation from aqueous media, *Process Saf. Environ. Prot.*, 129 (2019) 138–151.
- M. Malakootian, N. Olama, A. Nasiri, Photocatalytic degradation of metronidazole from aquatic solution by TiO<sub>2</sub>-doped Fe<sup>3+</sup> nano-photocatalyst, *Int. J. Environ. Sci. Technol.*, 16 (2019) 4275–4284.
- A. Nasiri, F. Tamaddon, M.H. Mosslemin, M. Faraji, A microwave assisted method to synthesize nanoCoFe<sub>2</sub>O<sub>4</sub>@methyl cellulose as a novel metal-organic framework for antibiotic degradation, *MethodsX*, 6 (2019) 1557–1563.
- A. Nasiri, F. Tamaddon, M.H. Mosslemin, M.A. Gharaghani, A. Asadipour, New magnetic nanobiocomposite CoFe<sub>2</sub>O<sub>4</sub>@methylcellulose: facile synthesis, characterization, and photocatalytic degradation of metronidazole, *J. Mater. Sci.: Mater. Electron.*, 30 (2019) 8595–8610.
- F. Tamaddon, M.H. Mosslemin, A. Asadipour, M.A. Gharaghani, A. Nasiri, Microwave-assisted preparation of ZnFe<sub>2</sub>O<sub>4</sub>@methyl cellulose as a new nano-biomagnetic photocatalyst for photodegradation of metronidazole, *Int. J. Biol. Macromol.*, 154 (2020) 1036–1049.
- F. Tamaddon, A. Nasiri, G. Yazdanpanah, Photocatalytic degradation of ciprofloxacin using CuFe<sub>2</sub>O<sub>4</sub>@methyl cellulose based magnetic nanobiocomposite, *MethodsX*, 7 (2020) 100764, <https://doi.org/10.1016/j.mex.2019.12.005>.
- R.S. Bangari, N. Sinha, Adsorption of tetracycline, ofloxacin and cephalexin antibiotics on boron nitride nanosheets from aqueous solution, *J. Mol. Liq.*, 293 (2019) 111376.
- N. Javid, A. Nasiri, M. Malakootian, Removal of nonylphenol from aqueous solutions using carbonized date pits modified with ZnO nanoparticles, *Desal. Water Treat.*, 141 (2019) 140–148.
- M. Malakootian, M. Hashemi, A. Toolabi, A. Nasiri, Investigation of nickel removal using poly(amidoamine) generation 4 dendrimer (PAMAM G4) from aqueous solutions, *J. Eng. Res.*, 6 (2018).
- M. Malakootian, A. Nasiri, H. Mahdizadeh, Preparation of CoFe<sub>2</sub>O<sub>4</sub>/activated carbon@chitosan as a new magnetic nanobiocomposite for adsorption of ciprofloxacin in aqueous solutions, *Water Sci. Technol.*, 78 (2018) 2158–2170.
- M. Malakootian, A. Nasiri, H. Mahdizadeh, Metronidazole adsorption on CoFe<sub>2</sub>O<sub>4</sub>/activated carbon@chitosan as a new magnetic biocomposite: modelling, analysis, and optimization by response surface methodology, *Desal. Water Treat.*, 164 (2019) 215–227.
- M. Dehghani, M. Nozari, A. Fakhraei Fard, M. Ansari Shiri, N. Shamsedini, Direct red 81 adsorption on iron filings from aqueous solutions; kinetic and isotherm studies, *Environ. Technol.*, 40 (2019) 1705–1713.
- M. Dehghani, M. Ansari Shiri, S. Shahsavani, N. Shamsedini, M. Nozari, Removal of Direct Red 81 dye from aqueous solution using neutral soil containing copper, *Desal. Water Treat.*, 86 (2017) 213–220.
- M. Dehghani, M. Nozari, I. Golkari, N. Rostami, M.A. Shiri, Adsorption and kinetic studies of hexavalent chromium by

- dehydrated *Scrophularia striata* stems from aqueous solutions, *Desal. Water Treat.*, 125 (2018) 81–92.
- [32] M. Maqbool, H.N. Bhatti, S. Sadaf, M.M. AL-Anazy, M. Iqbal, Biocomposite of polyaniline and sodium alginate with *Oscillatoria* biomass: a potential adsorbent for the removal of basic blue 41, *J. Mater. Res. Technol.*, 9 (2020) 14729–14741.
- [33] S. Nausheen, H.N. Bhatti, K. Arif, J. Nisar, M. Iqbal, Native clay,  $MnFe_2O_4$ /clay composite and bio-composite efficiency for the removal of synthetic dye from synthetic solution: column versus batch adsorption studies, *Desal. Water Treat.*, 187 (2020) 219–231.
- [34] H.N. Bhatti, Y. Safa, S.M. Yakout, O.H. Shair, M. Iqbal, A. Nazir, Efficient removal of dyes using carboxymethyl cellulose/alginate/polyvinyl alcohol/rice husk composite: adsorption/desorption, kinetics and recycling studies, *Int. J. Biol. Macromol.*, 150 (2020) 861–870.
- [35] S. Noreen, H.N. Bhatti, M. Iqbal, F. Hussain, F.M. Sarim, Chitosan, starch, polyaniline and polypyrrole biocomposite with sugarcane bagasse for the efficient removal of Acid Black dye, *Int. J. Biol. Macromol.*, 147 (2020) 439–452.
- [36] C. Gérente, P.C. Du Mesnil, Y. Andrès, J.-F. Thibault, P. Le Cloirec, Removal of metal ions from aqueous solution on low cost natural polysaccharides: sorption mechanism approach, *React. Funct. Polym.*, 46 (2000) 135–144.
- [37] A.B. Nasr, K. Walha, C. Charcosset, R.B. Amar, Removal of fluoride ions using cuttlefish bones, *J. Fluorine Chem.*, 132 (2011) 57–62.
- [38] M. Keshtkar, S. Dobaradaran, I. Nabipour, A.H. Mahvi, F.F. Ghasemi, Z. Ahmadi, M. Heydari, Isotherm and kinetic studies on fluoride biosorption from aqueous solution by using cuttlebone obtained from the Persian Gulf, *Fluoride*, 49 (2016) 343–351.
- [39] H. Khazri, I. Ghorbel-Abid, R. Kalfat, M. Trabelsi-Ayadi, Removal of drugs by cuttlefish bone powder: equilibrium, kinetics and thermodynamic study, *J. Environ. Anal. Chem.*, 3 (2016) 2.
- [40] P. Wang, X. Wang, S. Yu, Y. Zou, J. Wang, Z. Chen, N.S. Alharbi, A. Alsaedi, T. Hayat, Y. Chen, Silica coated  $Fe_3O_4$  magnetic nanospheres for high removal of organic pollutants from wastewater, *Chem. Eng. J.*, 306 (2016) 280–288.
- [41] N.M. Mohammadi Amini, E. Dehghanifard, Evaluation the efficiency of magnetic-metallic chitosan nanocomposite adsorbent in the removal of tetracycline antibiotic from aqueous solutions, *J. Environ. Health Eng.*, 6 (2019) 356–374.
- [42] S.T. Danalioğlu, Ş.S. Bayazit, Ö.K. Kuyumcu, M.A. Salam, Efficient removal of antibiotics by a novel magnetic adsorbent: magnetic activated carbon/chitosan (MACC) nanocomposite, *J. Mol. Liq.*, 240 (2017) 589–596.
- [43] S.T. Danalioğlu, Ö.K. Kuyumcu, M.A. Salam, Ş.S. Bayazit, Chitosan grafted  $SiO_2-Fe_3O_4$  nanoparticles for removal of antibiotics from water, *Environ. Sci. Pollut. Res.*, 25 (2018) 36661–36670.
- [44] B. Yu, Y. Bai, Z. Ming, H. Yang, L. Chen, X. Hu, S. Feng, S.-T. Yang, Adsorption behaviors of tetracycline on magnetic graphene oxide sponge, *Mater. Chem. Phys.*, 198 (2017) 283–290.
- [45] V. Arya, L. Philip, Adsorption of pharmaceuticals in water using  $Fe_3O_4$  coated polymer clay composite, *Microporous Mesoporous Mater.*, 232 (2016) 273–280.
- [46] Y. Lin, S. Xu, J. Li, Fast and highly efficient tetracyclines removal from environmental waters by graphene oxide functionalized magnetic particles, *Chem. Eng. J.*, 225 (2013) 679–685.
- [47] J. Yu, W. Xiong, X. Li, Z. Yang, J. Cao, M. Jia, R. Xu, Y. Zhang, Functionalized MIL-53 (Fe) as efficient adsorbents for removal of tetracycline antibiotics from aqueous solution, *Microporous Mesoporous Mater.*, 290 (2019) 109642.
- [48] J. Che, J. Wan, X. Huang, R. Wu, K. Liang, Pretreatment of piggy digestate wastewater by ferric-carbon micro-electrolysis under alkaline condition, *Korean J. Chem. Eng.*, 34 (2017) 2397–2405.
- [49] H. Zhou, Y. Shen, P. Lv, J. Wang, J. Fan, Degradation of 1-butyl-3-methylimidazolium chloride ionic liquid by ultrasound and zero-valent iron/activated carbon, *Sep. Sci. Technol.*, 104 (2013) 208–213.
- [50] M. Behloul, H. Grib, N. Drouiche, N. Abdi, H. Lounici, N. Mameri, Removal of malathion pesticide from polluted solutions by electrocoagulation: modeling of experimental results using response surface methodology, *Sep. Sci. Technol.*, 48 (2013) 664–672.
- [51] S. Demim, N. Drouiche, A. Aouabed, S. Semsari, CCD study on the ecophysiological effects of heavy metals on *Lemma gibba*, *Ecol. Eng.*, 57 (2013) 302–313.
- [52] S.K. Behera, H. Meena, S. Chakraborty, B. Meikap, Application of response surface methodology (RSM) for optimization of leaching parameters for ash reduction from low-grade coal, *Int. J. Min. Sci. Technol.*, 28 (2018) 621–629.
- [53] H. Amiri, R. Nabizadeh, S.S. Martinez, S.J. Shahtaheri, K. Yaghmaeian, A. Badii, S. Nazmara, K. Naddafi, Response surface methodology modeling to improve degradation of *Chlorpyrifos* in agriculture runoff using  $TiO_2$  solar photocatalytic in a raceway pond reactor, *Ecotoxicol. Environ. Saf.*, 147 (2018) 919–925.
- [54] S. Ahmadzadeh, A. Asadipour, M. Pournamdari, B. Behnam, H.R. Rahimi, M. Dolatabadi, Removal of ciprofloxacin from hospital wastewater using electrocoagulation technique by aluminum electrode: optimization and modelling through response surface methodology, *Process Saf. Environ. Prot.*, 109 (2017) 538–547.
- [55] M. Leili, M. Fazlzadeh, A. Bhatnagar, Green synthesis of nano-zero-valent iron from Nettle and Thyme leaf extracts and their application for the removal of cephalixin antibiotic from aqueous solutions, *Environ. Technol.*, 39 (2018) 1158–1172.
- [56] M. Dehghani, M. Nozari, I. Golkari, N. Rostami, M. Ansari Shiri, Adsorption of mercury(II) from aqueous solutions using dried *Scrophularia striata* stems: adsorption and kinetic studies, *Desal. Water Treat.*, 203 (2020) 279–291.
- [57] K. Kaneko, Determination of pore size and pore size distribution: 1. Adsorbents and catalysts, *J. Membr. Sci.*, 96 (1994) 59–89.
- [58] S. Dobaradaran, I. Nabipour, M. Keshtkar, F.F. Ghasemi, T. Nazarialamdarloo, F. Khalifeh, M. Poorhosein, M. Abtahi, R. Saeedi, Self-purification of marine environments for heavy metals: a study on removal of lead(II) and copper(II) by cuttlebone, *Water Sci. Technol.*, 75 (2017) 474–481.
- [59] M. Dehvari, M.H. Ehrampoush, M.T. Ghaneian, B. Jamshidi, M. Tabatabaee, Adsorption kinetics and equilibrium studies of reactive red 198 dye by cuttlefish bone powder, *Iran J. Chem. Chem. Eng.*, 36 (2017) 143–151.
- [60] J. He, F. Ni, A. Cui, X. Chen, S. Deng, F. Shen, C. Huang, G. Yang, C. Song, J. Zhang, D. Tian, L. Long, Y. Zhu, L. Luo, New insight into adsorption and co-adsorption of arsenic and tetracycline using a Y-immobilized graphene oxide-alginate hydrogel: adsorption behaviours and mechanisms, *Sci. Total Environ.*, 701 (2020) 134363, <https://doi.org/10.1016/j.scitotenv.2019.134363>.
- [61] M. Foroughi, M.H.A. Azghandi, S. Kakhki, Bio-inspired, high, and fast adsorption of tetracycline from aqueous media using  $Fe_3O_4$ -g-CN@PEI- $\beta$ -CD nanocomposite: modeling by response surface methodology (RSM), boosted regression tree (BRT), and general regression neural network (GRNN), *J. Hazard. Mater.*, 388 (2020) 121769.
- [62] A.A. Maryoosh, M.A. Abed, A.A. Waheb, R.F. Abbas, H.K. Hami, Isotherm and pH effect studies of tetracycline drug removal from aqueous solution using cobalt oxide surface, *Al-Nahrain J. Sci.*, 22 (2019) 12–18.
- [63] A.A. Mohammed, S.L. Kareem, Adsorption of tetracycline from wastewater by using Pistachio shell coated with ZnO nanoparticles: equilibrium, kinetic and isotherm studies, *Alexandria Eng. J.*, 58 (2019) 917–928.
- [64] G. Yang, Q. Gao, S. Yang, S. Yin, X. Cai, X. Yu, S. Zhang, Y. Fang, Strong adsorption of tetracycline hydrochloride on magnetic carbon-coated cobalt oxide nanoparticles, *Chemosphere*, 239 (2020) 124831.
- [65] H. Zhu, T. Chen, J. Liu, D. Li, Adsorption of tetracycline antibiotics from an aqueous solution onto graphene oxide/calcium alginate composite fibers, *RSC Adv.*, 8 (2018) 2616–2621.

- [66] D. Balarak, Y. Mahdavi, F.K. Mostafapour, Application of alumina-coated carbon nanotubes in removal of tetracycline from aqueous solution, *J. Pharm. Res. Int.*, 12 (2016) 1–11.
- [67] U.A. Guler, M. Sarioglu, Removal of tetracycline from wastewater using pumice stone: equilibrium, kinetic and thermodynamic studies, *J. Environ. Health Sci. Eng.*, 12 (2014) 79.
- [68] C. Zhao, J. Ma, Z. Li, H. Xia, H. Liu, Y. Yang, Highly enhanced adsorption performance of tetracycline antibiotics on KOH-activated biochar derived from reed plants, *RSC Adv.*, 10 (2020) 5066–5076.
- [69] J. Wei, Y. Liu, J. Li, Y. Zhu, H. Yu, Y. Peng, Adsorption and co-adsorption of tetracycline and doxycycline by one-step synthesized iron loaded sludge biochar, *Chemosphere*, 236 (2019) 124254, <https://doi.org/10.1016/j.chemosphere.2019.06.224>.
- [70] Y. Dai, J. Li, D. Shan, Adsorption of tetracycline in aqueous solution by biochar derived from waste *Auricularia auricula* dregs, *Chemosphere*, 238 (2020) 124432, <https://doi.org/10.1016/j.chemosphere.2019.124432>.
- [71] V. Rizzi, D. Lacalamita, J. Gubitosa, P. Fini, A. Petrella, R. Romita, A. Agostiano, J.A. Gabaldón, M.I.F. Gorbe, T. Gómez-Morte, Removal of tetracycline from polluted water by chitosan-olive pomace adsorbing films, *Sci. Total Environ.*, 693 (2019) 133620.
- [72] V.T. Nguyen, T.B. Nguyen, C.W. Chen, C.M. Hung, C. Huang, C.D. Dong, Cobalt-impregnated biochar (Co-SCG) for heterogeneous activation of peroxymonosulfate for removal of tetracycline in water, *Bioresour. Technol.*, 292 (2019) 121954.
- [73] J. Liu, B. Zhou, H. Zhang, J. Ma, B. Mu, W. Zhang, A novel Biochar modified by Chitosan-Fe/S for tetracycline adsorption and studies on site energy distribution, *Bioresour. Technol.*, 294 (2019) 122152.
- [74] W. Xiong, Z. Zeng, G. Zeng, Z. Yang, R. Xiao, X. Li, J. Cao, C. Zhou, H. Chen, M. Jia, Metal-organic frameworks derived magnetic carbon- $\alpha$ Fe/Fe<sub>3</sub>C composites as a highly effective adsorbent for tetracycline removal from aqueous solution, *Chem. Eng. J.*, 374 (2019) 91–99.
- [75] Y. Gao, Y. Li, L. Zhang, H. Huang, J. Hu, S.M. Shah, X. Su, Adsorption and removal of tetracycline antibiotics from aqueous solution by graphene oxide, *J. Colloid Interface Sci.*, 368 (2012) 540–546.
- [76] W. Xiong, Z. Zeng, X. Li, G. Zeng, R. Xiao, Z. Yang, Y. Zhou, C. Zhang, M. Cheng, L. Hu, Multi-walled carbon nanotube/amino-functionalized MIL-53 (Fe) composites: remarkable adsorptive removal of antibiotics from aqueous solutions, *Chemosphere*, 210 (2018) 1061–1069.